# Two-channel competition of autoionizing Rydberg states in an electric field

J. B. M. Warntjes, C. Nicole, F. Rosca-Pruna, I. Sluimer, M. J. J. Vrakking,
and L. D. Noordam
*FOM-Institute for Atomic and Molecular Physics (AMOLF), Kruislaan 407, 1098 SJ Amsterdam, The Netherlands*

F. Robicheaux
*Department of Physics, Auburn University, Auburn, Alabama 36849*
(Received 5 July 2000; published 11 April 2001)

We present experimental data on the decay of xenon Stark states converging to the upper spin limit. In an electric field the Rydberg electron has two qualitatively different decay paths. If the electron changes the core state from the upper spin state into the lower spin state, it gains sufficient energy to escape the ionic core and autoionizes. Moreover, if the electronic state is above the saddle point, created by the electric field, it can field ionize. The probability to autoionize is nearly constant around the saddle point whereas the probability to field ionize rapidly increases above the saddle point. With the velocity map imaging technique we monitor both ionization channels as a function of (increasing) photoexcitation energy. We observe that the field ionization channel dominates the competition and gains yield at the expense of the autoionization channel. The spectra are explained both with full quantum calculations and with a relatively simple description for the overall behavior. These experiments show that the field ionization can be used in general as a clock for total core-dependent decay.

DOI: 10.1103/PhysRevA.63.053403 PACS number(s): 32.80.Rm, 32.80.Dz, 32.60.+i

## I. INTRODUCTION

Decay of a highly excited electron most often occurs through interaction with the ionic core. The rate of, e.g., rotational and vibrational autoionization, fluorescence and predissociation is proportional to the frequency with which an electron returns to the vicinity of the ionic core. Throughout the Rydberg series the ratio between these decay channels remains constant. In this respect field ionization is a special decay channel. A static electric field distorts the Coulomb potential by raising the potential in the direction of the field and lowering it on the other side. The maximum on the down-potential side is called the saddle point. An electron that is excited above the saddle point is energetically allowed to escape from the ionic core. The rate for electron emission depends strongly on the opening angle at which the electron can escape. This opening angle rapidly increases above the saddle point making the field ionization change from zero to the dominant pathway of decay in a small energy range. How rapidly the field ionization dominates depends on the competition with the core-dependent decay. This competition is reflected in the overall behavior of the ionization spectra, allowing one to retrieve the rate of one channel with the spectrum of the other.

In a recent paper we investigated the field ionization yield above the saddle point energy of nitric oxide in a strong electric field [1]. A competition between the field ionization and predissociation of the NO molecule is observed. The field ionization yield just above the saddle point was strongly reduced by the other decay channel and the ionization threshold appeared to have shifted to higher energy. Computing the field ionization spectrum yielded the rate of predissociation. In that experiment only the field ionization channel was monitored. To investigate a two-channel competition properly, however, one wants to monitor the two channels simultaneously. An ideal system of investigation is the autoionization from the Rydberg states converging to the upper spin state of a noble gas in a strong electric field. The field ionized electrons have nearly zero kinetic energy whereas the electrons that autoionize by changing the core spin-orbit state, carry a kinetic energy of 1–2 eV, which makes the two ionization channels separable. The two channels are distinguished by velocity map imaging. The detected spectra, as presented in Sec. III, are simulated by full quantum calculations based on multichannel Stark theory [1–3]. Moreover, we show that the overall behavior of the spectra can already be simulated by relative simple rate equations. In Sec. IV we derive these equations and compare with the experimental observations.

## II. EXPERIMENTAL SCHEME

Xenon is chosen to monitor the competition between field ionization and autoionization. The spin-flip energy is 1.3 eV. A difficulty, however, is the high excitation energy. This is overcome by populating highly excited, metastable states of the Xe atoms by electron impact. The excitation scheme is shown in Fig. 1. The metastable states are the $6s'$ $(J=0)$ at 76197.3 $cm^{-1}$ and $6s$ $(J=2)$ at 67068.0 $cm^{-1}$ above the ground state [4], where $J$ is the total angular momentum. The electron is optically excited to Rydberg states converging to the ion with $J_{ion}=1/2$ at 108371.4 $cm^{-1}$ above the ground state, and the states converging to the ion with $J_{ion}=3/2$ at 97834.4 $cm^{-1}$ [4] . With a typical field strength of 900 V/cm and excitation energy of 32174 $cm^{-1}$ an electron in the $J_{ion}=1/2$ channel can be field ionized (FI) with nearly zero kinetic energy. Configuration interaction (CI) by spin orbit coupling between the two channels results in autoionization (AI). An autoionized electron carries an excess kinetic energy of 10 537 $cm^{-1}$ (1.3 eV). The energy differ-

 

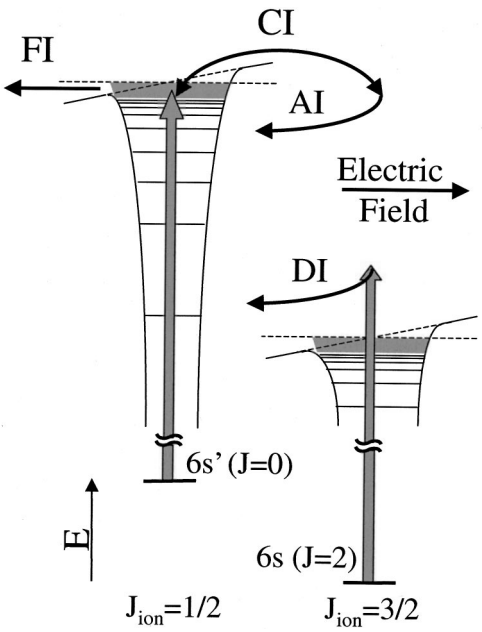


FIG. 1. Excitation scheme of the two-channel measurements. There are two initial metastable states, $6s'$ $(J=0)$ and $6s$ $(J=2)$, that are excited with an optical pulse. In the $J_{\text{ion}}=1/2$ channel the electron is promoted to a highly excited Rydberg state. Above the saddle point the electron can be field ionized (FI). The $J_{\text{ion}}=1/2$ channel is coupled to the $J_{\text{ion}}=3/2$ channel by configuration interaction (CI). If the spin state of the ionic core is changed the excess energy is donated to the electron that autoionizes (AI). The initial state in the $J_{\text{ion}}=3/2$ channel is somewhat higher in energy compared to its ionization limit than the one in the $J_{\text{ion}}=1/2$ channel. Laser excitation results in direct ionization (DI) of the electron into the continuum.

ence between the two metastable states is smaller than between the two ionization limits. The same laser excitation from the $6s$ $(J=2)$ metastable state will result in direct ionization (DI) into the continuum of the $J_{\text{ion}}=3/2$ channel. The excess kinetic energy of the directly ionized electron is in this case 1408 $\text{cm}^{-1}$. Upon laser excitation of 32 174 $\text{cm}^{-1}$ we thus have to distinguish between electrons of three different kinetic energies 0 (FI of the upper spin state), 1408 (DI of the lower spin state), and 10 537 $\text{cm}^{-1}$ (AI from the upper spin state). Note that the DI process is independent of the two other processes since it is due to the decay of another excited state.

The experimental set-up is depicted in Fig. 2. A jet of Xe is produced by a pulsed valve with a backing pressure of 2 bar. The gas is led through a hot, tungsten filament [5]. Electrons from the filament are accelerated along the Xe beam by a repeller, electron optics, and an electromagnet. Xe is excited to several metastable states by the electron bombardment. Charged particles are separated from the neutral beam by deflection plates. Only the $6s'$ $(J=0)$ and $6s$ $(J=2)$ metastable states survive the time of flight ($\sim\mu$s) to the interaction region, with an observed population ratio of 1:10. In the interaction region the atoms are subject to a variable, static electric field between a repeller plate and an extractor. The optical excitation with a narrowband laser around 32 174

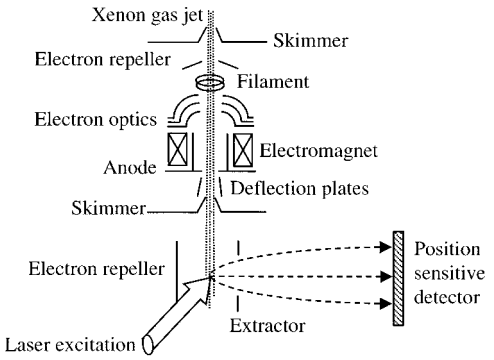


FIG. 2. Schematic outline of the experimental setup. A xenon gas jet is led through a hot tungsten filament and two skimmers. Electron bombardment, guided by a set of electron optics and an electromagnet, excites the Xe atoms to metastable states. Charged particles are separated from the neutral beam by deflection plates. The metastable Xe is futher excited by laser light, with a polarization perpendicular to the electric field in the interaction region. Electrons that ionize are accelerated towards a position sensitive detector by means of a repeller plate and an extractor ring. The position of the electron signal depends on the kinetic energy of the electron perpendicular to the electric field.

$\text{cm}^{-1}$ is done in two ways (i) A Quanta-ray Nd:YAG laser pumped Scanmate Dye laser produces pulses around 622 nm (16 077 $\text{cm}^{-1}$) with an energy of 5 mJ, a duration of 7 ns and a bandwidth of 0.2 $\text{cm}^{-1}$. The laser pulse is frequency doubled with a KDP-R6G crystal to populate Rydberg states with a one-photon excitation. (ii) An alternative way to excite the electron is to tune the same dye laser to around 747 nm (13 387 $\text{cm}^{-1}$) and send the pulse to the interaction region collinear with the second harmonic of the Nd:YAG laser (532.2 nm or 18 790 $\text{cm}^{-1}$, with a bandwidth of 0.5 $\text{cm}^{-1}$, referred to as ''Nd:YAG'' from now on) in a $1+1'$ excitation scheme [6].

In an electric field of typically 200–1000 V/cm the kinetic energy difference of 1.3 eV between a field ionized electron and an autoionized electron cannot easily be distinguished by time of flight. However, velocity map imaging [7,8] is excellently suited to measure kinetic energy differences in the presence of a strong electric field. The polarization of the excitation laser is chosen perpendicular to the electric field. The electrons that autoionize carry an excess kinetic energy perpendicular to the direction of the electric field. The outgoing electron density is accelerated towards a position sensitive imaging detector consisting of a set of multichannel plates and phosphor screen, viewed by a CCD camera. The CCD image shows a two-dimensional projection of the electron probability at a particular time (the arrival time at the detector) after ionization.

## III. RESULTS AND DISCUSSION

Figure 3 shows a typical CCD image of the velocity map imaging. The electric field is 900 V/cm. The photo excitation is just above the saddle point, with a polarization perpendicular to the electric field (along the *x* axis of the image in Fig. 3). The strong dot in the center of the image corresponds

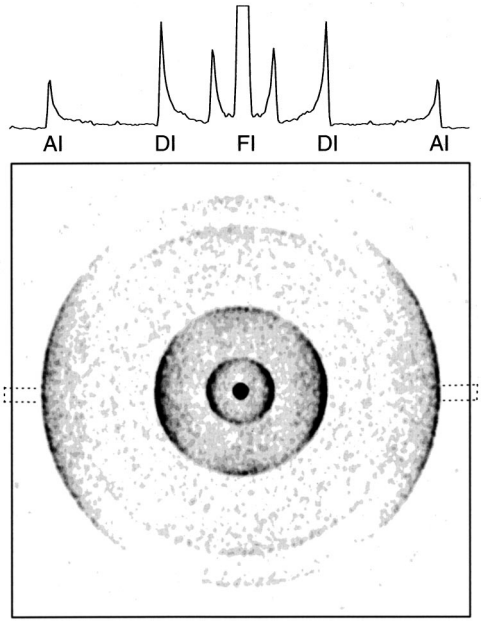


FIG. 3. A typical image of velocity map imaging. The central spot with the field ionization signal (FI) is very intense and off scale. The small inner ring is a fraction of the field ionization signal that has scattered off the ionic core. The large inner ring is the direct ionization (DI) and the outer ring corresponds to the autoionization (AI). On top a horizontal slice through the middle of the image is shown.

to the field ionization (FI) yield. The small inner ring is a fraction of the field ionization that has scattered of the ionic core. The intensity of such a ring is less than 10% of that of the central dot. The large inner ring corresponds to direct ionization (DI) and the outer ring to autoionization (AI). Shown on top of the image is a horizontal slice through the middle of the image. Velocity map imaging is based on the relation between the excess kinetic energy of an electron perpendicular to the direction of the electric field and the radius of the ring of electron signal on the CCD image. The maximum radius is proportional to the square root of the kinetic energy. Only at very low energies, up to 200 $cm^{-1}$, does the radius exhibit a more complicated function of kinetic energy, as is seen with the field ionization in Fig. 3. A more detailed discussion about the angular distribution of electron density on the image and the features at low kinetic energy is beyond the scope of this article and will be described more thoroughly in a forthcoming article [9].

The radial electron density distribution is obtained by angularly integrating the electron signal as a function of distance from the center of the image. Figure 4 shows the radial distributions of ionization yield upon various excitation wavelengths in a field of 900 V/cm. The spectra are plotted as a function of the number of pixels from the center of the images. As a test experiment only the second harmonic Nd:YAG photons with an energy of 18 790 $cm^{-1}$ are used. The detected radial distribution is shown in the lower trace of Fig. 4. The strongest feature (e) results from two photon ionization in the $J_{ion}=3/2$ channel, yielding a kinetic energy of 6814 $cm^{-1}$ above the zero-field ionization limit of 97 834

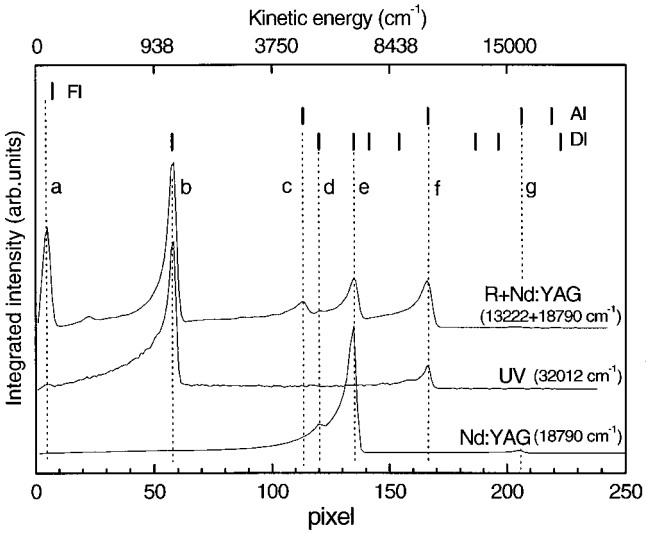


FIG. 4. Radial distribution of electron yield of the velocity map imaging upon various excitations. Metastable Xe is excited with the second harmonic of a Nd:YAG laser at 18 790 $cm^{-1}$ (532.2 nm; Nd:YAG), with an ultraviolet pulse of 32 012 $cm^{-1}$ (312.4 nm; UV) or with simultaneously a red pulse at 13 222 $cm^{-1}$ (756.3 nm; R) with the second harmonic of a Nd:YAG laser. The electric field is 900 V/cm. Indicated on top are the expected maximum radii of field ionization (FI), autoionization (AI) and direct ionization (DI), based on the involved excitation energies and an empirical $c=0.375$. The most prominent features are denoted (a) field ionization in the $J_{ion}=1/2$ channel. (b) Direct ionization in the $J_{ion}=3/2$ channel. (c) Autoionization from the $J_{ion}=1/2$ channel to the $J_{ion}=3/2$ channel with two red photons. (d) Direct ionization in the $J_{ion}=1/2$ channel with two Nd:YAG photons. (e) Direct ionization in the $J_{ion}=3/2$ channel with two Nd:YAG photons. (f) Autoionization from the $J_{ion}=1/2$ channel to the $J_{ion}=3/2$ channel.

$cm^{-1}$. The small features at pixel 120 and 205 are, respectively, direct ionization in the $J_{ion}=1/2$ channel (d) and direct ionization from the $6s'$ $(J=0)$ state into the $J_{ion}=3/2$ channel (g).

Excitation with an ultraviolet pulse of 32012 $cm^{-1}$ (UV) results in the radial distribution that is shown in the middle trace of Fig. 4. Feature (a) is field ionization in the $J_{ion}=1/2$ channel, feature (f) is autoionization from the $J_{ion}=1/2$ channel to the $J_{ion}=3/2$ channel and feature (b) is direct ionization in the $J_{ion}=3/2$ channel. Conversion to kinetic energy $E_{kin}$ of the electron (the component perpendicular to the electric field) is obtained by

$$E_{kin}=c*(\text{pixel})^2, \tag{1}$$

where $c$ is an experimental value depending on the fields used and distances of the phosphor screen and CCD camera from the interaction region. In this case $c=0.375$ $cm^{-1}$. At the maximum radius of the signal the kinetic energy component perpendicular to the electric field is equal to the total kinetic energy of the electron. There are two reasons not to plot energy on the $x$ axis in Fig. 4. Firstly, the high-energy side of the spectra becomes stretched so much that it becomes hard to see the low-energy side. Secondly, there is the question of the binding energy of the electron. Starting with

a metastable state the electron has a certain binding energy to overcome in order to ionize. For direct ionization the binding energy is the zero-field ionization energy. If the electron scatters of the core and field ionizes the binding energy is the saddle point energy, which is 183 $cm^{-1}$ lower in a field of 900 V/cm. The difference is small at the high energies around 15000 $cm^{-1}$. At low energies, however, the difference becomes important and one would expect the peak at (b) at pixel 61 instead of 57 if one assumes the saddle point energy (rather than the zero-field energy) as binding energy.

For the two-channel competition experiments we chose to excite the Xe metastable states with a combination of a red pulse around 13 222 $cm^{-1}$ ($R$) with the second harmonic of a Nd:YAG laser (18 970 $cm^{-1}$). The radial distribution of electron yield is shown in the upper graph in Fig. 4. There are two advantages of this excitation scheme over single-photon excitation of the metastable states by a UV pulse: As can be seen in Fig. 4 the relative intensity of the FI and AI signals [features (a) and (f)] as compared to the DI signal (b) greatly enhances upon using the $R$+Nd:YAG combination. The electron yield of (a) and (f) is increased with the help of the $6p'$ $J=1$ state at 89 279 $cm^{-1}$. Although about 140 $cm^{-1}$ off resonance, the large oscillator strength of the $6p'$ state relatively enhances the integrated yield from the field ionization FI and autoionization signal AI from the $J_{ion}$ = 1/2 channel to be equal to the direct ionization signal DI of the $J_{ion}=3/2$ channel. One new feature appears (c), which is attributed to photoionization of the metastable state in the $J_{ion}=1/2$ channel excited with two red photons, autoionizing into the $J_{ion}=3/2$ channel. The second reason to detect the FI and AI from the $J_{ion}=1/2$ channel with a combination of excitation lasers is that the autoionization from the $J_{ion}=1/2$ channel to the $J_{ion}=3/2$ channel [$|D_{AI}|^2$ in Eq. (3) in Sec. IV] in case of UV excitation is always strong; the AI signal remains more or less constant upon increasing excitation energy above the saddlepoint energy. We have no explanation for the large $|D_{AI}|^2$ in this particular case.

Integration windows are set over the FI, DI, and AI signals and the total electron yield is monitored as a function of the excitation energy. The windows are set at 0–15, 16–65, and 140–170 pixels, respectively. We assume that the DI signal is frequency independent and first divide the FI and AI signals by the DI yield in order to remove intensity fluctuations of the laser. In Fig. 5(a) the observed integrated electron yield from the field ionization is shown as a function of the energy of one red plus one Nd:YAG photon. The saddle-point at 900 V/cm is at 31 991 $cm^{-1}$. The FI electron yield is increasing over an energy range of about 25 $cm^{-1}$ above the saddle point. Simultaneously the AI signal is decreasing as shown in Fig. 5(b). Note that the Stark structure is well resolved. The observed spacing between the states is 3.1 $cm^{-1}$. The $n=26$ manifold is expected to be around 32 012 $cm^{-1}$. In a field of 900 V/cm the hydrogenic spacing between the Stark states of $n=26$ is 3.0 $cm^{-1}$ corresponding well with the observed spacing. There is a strong resonance in the AI signal at 32 008 $cm^{-1}$ seen in Fig. 5(b). This is, however, an experimental artifact: In the radial distribution (not shown) is seen that at this wavelength two new rings appear, one of which falls in the AI window [10].

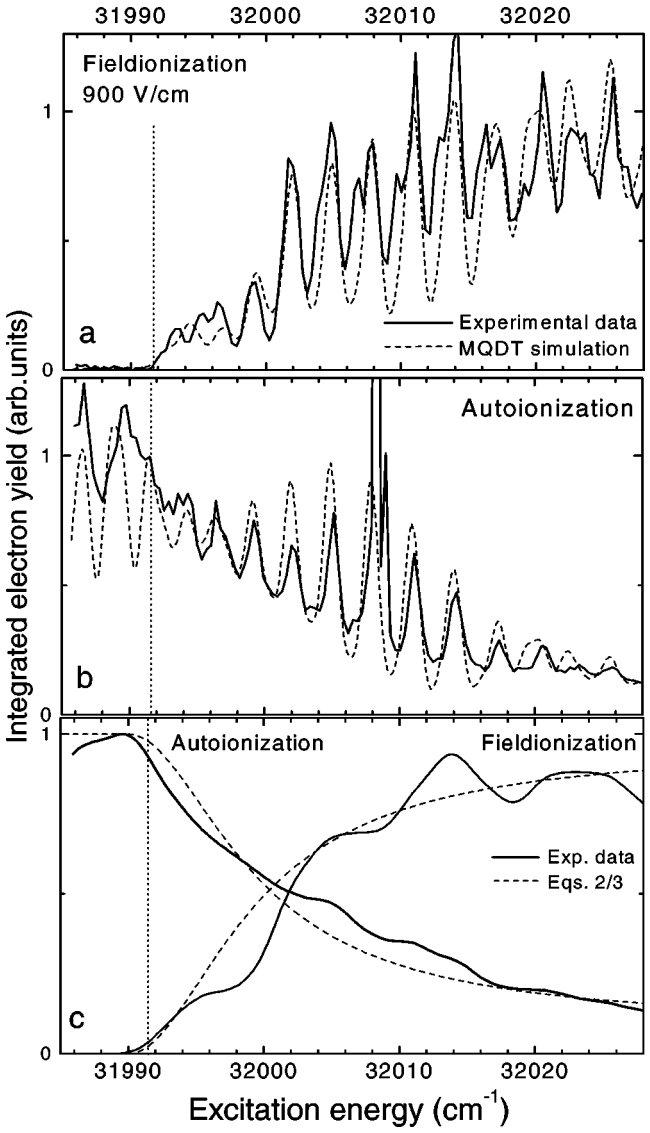


FIG. 5. (a) Integrated electron yield of field ionization (FI) in the $J_{ion}=1/2$ channel as a function of the energy of one red and one Nd:YAG photon of 18 790 $cm^{-1}$. The saddle point energy for the $J_{ion}$ = 1/2 channel at 900 V/cm is 31 991 $cm^{-1}$ above the metastable state in the $J_{ion}=1/2$ channel. The dashed line shows the simulation based on a full quantum calculation (see text). (b) Same for autoionization (AI) from the $J_{ion}=1/2$ channel to the $J_{ion}=3/2$ channel. (c) Both experimental spectra, convoluted with a Gaussian of 2 $cm^{-1}$. The dashed line is the overall behavior based on Eqs. (2) and (3) with $S_{AI}$ = 0.17 and $|D_{AI}|^2=0.05$.

Also plotted in Figs. 5(a) and 5(b) are the theoretical fits based on a full MQDT calculation. The Stark structure is well reproduced. Adding the two spectra results in the absorption cross section. The calculations are based on the method described in detail in Ref. [3], giving the details for obtaining the outgoing wave functions and dipole matrix elements for multichannel atoms in a static electric field. The method uses zero-field channel coupling matrices and the transformation amplitudes from spherical-to-parabolic wave functions to obtain the full multichannel wave function in the static electric field. For the competition studied here, we cal-

culated all of the zero-field channel coupling matrices for Xe using an *R*-matrix calculation in LS coupling; the *jj*-coupled channel interactions were computed through an LS-*jj* frame transformation and the K-matrices were empirically modified at the few percent level to improve agreement with the zero field, experimental energies. The two-photon dipole matrix elements in zero field were estimated by treating the absorption as only affecting the $6s$ electron in the initial state; it is most likely the dipole matrix elements are the least accurate part of the calculation.

In addition to the spatial degrees of freedom of the escaping electron, there are three other important quantum numbers. $J_{\mathrm{ion}}$: the total angular momentum of the $Xe^+$ core, $Q$: the angular momentum that results from coupling the spin of the Rydberg electron to $J_{\mathrm{ion}}$ of the core, and $M_q$: the projection of $Q$ on the $z$ axis. The initial state of Xe can be described as $5p^5\ {}^2P_{1/2}\ 6s\ J=0$ with an equal population in each $M$ level. The initial state has $J_{\mathrm{ion}}=1/2$, $Q=0$, $M_q=0$. The initial excitation mostly populates autoionizing states attached to the $J_{\mathrm{ion}}=1/2$ threshold because the photon mainly acts on the outer $6s$ electron. When the electron is near the core, the channel interactions allows the Rydberg electron to gain energy from the core and be ejected from the atom.

In Fig. 5(c) the same experimental spectra are depicted as in Figs. 5(a) and 5(b), but convoluted with a Gaussian of 2 $\mathrm{cm}^{-1}$(solid lines). The aim is to focus on the overall behavior of the electron yield. Above the saddlepoint, field ionization becomes possible. In the absence of autoionization the onset of electron yield of field ionization would be a sharp step function, exactly on the saddle point energy. Coupling between the two channels $J_{\mathrm{ion}}=1/2$ and $J_{\mathrm{ion}}=3/2$ quenches the field ionization intensity close to the saddle point. A slow rise of field ionization and a slow decrease of autoionization above the saddle point is observed. The exact overall behavior of the spectra depends on the competition between the two channels. Instead of a full MQDT simulation of the spectra, a good, qualitative picture of the overall behavior of the spectra as shown in Fig. 5(c) can already be obtained using an approximate description.

## IV. SIMULATION OF OVERALL BEHAVIOR

The photoionization spectra in a static field are very complicated so it may be somewhat surprising that the average behavior can be described by simple equations involving zero field parameters and the energy above the classical ionization threshold [1]. To simulate the overall behavior we assume that the spacings between Stark states of a single Rydberg manifold are not resolved. The basic idea is that by averaging over the Stark spacing almost all of the quantum standing wave behavior is lost. Therefore, the amount of flux into the field ionization channel or autoionization channel is given by the amount each partial wave scatters into each channel. This averaging is allowed because the partial waves are equally populated over the energy range and they each scatter independently. For some Stark resonance states, the partial waves scatter constructively but for other states they scatter destructively so that, on average, they behave as if they scatter independently.

The cross section of the field ionization $\sigma_{\mathrm{FI}}^F$, is described by

$$\sigma_{\mathrm{FI}}^F \propto |D_{\mathrm{FI}}|^2(\eta+[1-\eta]B_{\mathrm{FI}}), \tag{2}$$

where $D_{\mathrm{FI}}$ is the direct excitation amplitude in the $J_{\mathrm{ion}}=1/2$ channel and $\eta$ is the probability of direct ejection of the electron. The fraction that remains bound in the $J_{\mathrm{ion}}=1/2$ channel, $1\text{-}\eta$, recurs periodically to the ionic core and can still field ionize by scattering of the core with a branching ratio for field ionization $B_{\mathrm{FI}}$. The cross section of the autoionization $\sigma_{\mathrm{AI}}^F$ is

$$\sigma_{\mathrm{AI}}^F \propto |D_{\mathrm{AI}}|^2+|D_{\mathrm{FI}}|^2(1-\eta)(1-B_{\mathrm{FI}}), \tag{3}$$

where $D_{\mathrm{AI}}$ is the direct excitation amplitude into the autoionization channel.

There are two points to notice about these cross sections. The first that the sum of the field ionization and autoionization cross sections in the field equals the sum of the two cross sections in zero field. The second is that the field ionization cross section rapidly increases from zero to $|D_{\mathrm{FI}}|^2$ as the excitation energy increases from the saddlepoint at $-2\sqrt{F}$ to the zero-field ionization potential. The exact manner it increases depends on how well the electron can elastically scatter down potential compared to how well it can cause autoionization. That the competition between the two ionization channels is dominated at high excitation by the field ionization channel is obvious from the rapid decrease of the separatrix angle $\theta_s$ (which is $\pi$ minus the opening angle). An electron that leaves the region near the nucleus at an angle with respect to the $z$ axis larger than the separatrix angle can leave the atom and be counted as direct field ionization. The separatrix angle is given by

$$\sin(\theta_s/2)=-E/\sqrt{4F}=-\epsilon/2, \tag{4}$$

where $\epsilon$ is the scaled energy.

Both the probability for direct electron ejection $\eta$ and the branching ratio for field ionization $B_{\mathrm{FI}}$ depend on the function

$$\Phi_{\ell m}(\cos\theta_0)=2\pi\int_{-1}^{\cos\theta_0}|Y_{\ell m}|^2 d\cos\theta, \tag{5}$$

which is the fraction of the angular distribution in the range $\theta_0 \leqslant \theta \leqslant \pi$. For $\eta$ this is

$$\eta=\Phi_{\ell_0 m}(\cos\theta_s), \tag{6}$$

where $\ell_0$ is the initial orbital angular momentum of the outgoing electron. The branching ratio for field ionization $B_{\mathrm{FI}}$ is the probability for the electron to elastically scatter into the open region of space $S_{\mathrm{FI}}(\ell)$ divided by the sum of the probabilities to elastically scatter and to scatter into autoionization $S_{\mathrm{FI}}(\ell)+S_{\mathrm{AI}}(n\ell)$. We assume that the electric field thoroughly mixes the $\ell$'s of the bound fraction, so that all of

them are equally likely. For the $\ell$ partial wave, the probability to scatter and leave the molecule is

$$S_{\mathrm{FI}}(\ell) = 4\Phi_{\ell m}(\cos\theta_s)\sin^2(\pi\mu_\ell), \tag{7}$$

where $\mu_\ell$ is the quantum defect, and the probability to autoionize is

$$S_{\mathrm{AI}}(n\ell) = 2\pi(n-\mu_\ell)^3\Gamma_{\mathrm{AI}}(n\ell), \tag{8}$$

where $2\pi(n-\mu_\ell)^3$ is the Rydberg period in atomic units and $\Gamma_{\mathrm{AI}}(n\ell)$ is the zero field autoionization rate of the $n\ell$ state in atomic units. In terms of these parameters the branching ratio is

$$B_{\mathrm{FI}} = \sum_{\ell=|m|} S_{\mathrm{FI}}(\ell) \Big/ \sum_{\ell=|m|} [S_{\mathrm{FI}}(\ell) + S_{\mathrm{AI}}(\ell)]. \tag{9}$$

There is a fundamental limitation for using these formulas when the laser that excites the Rydberg electron is polarized in the direction of the field. For this case, $m=0$ and it is necessary to average over an energy range so that the standing wave on the $z$ axis is not resolved. This is usually too large an energy range to observe any interesting behavior in the average cross sections. Fortunately, the $m=0$ case is the least interesting one since so much of the elastically scattered wave travels directly down potential and leaves the atom: only over a small energy range just above the classical ionization threshold can autoionization compete with field ionization.

The dotted lines in Fig. 5(c) are theoretical predictions based on Eqs. (2) and (3). In the energy range from saddle point energy (31991 $\mathrm{cm}^{-1}$ in a field of 900 V/cm) to zero-field ionization potential (32174 $\mathrm{cm}^{-1}$) the term $S_{\mathrm{FI}}$ changes from 0 to 1. $S_{\mathrm{AI}}$, on the other hand, is a constant so that the branching ratio $B_{\mathrm{FI}}$ changes from 0 to $1/(S_{\mathrm{AI}}+1)$. The best result is obtained with $S_{\mathrm{AI}}=0.17\pm0.05$ and $|D_{\mathrm{AI}}|^2=0.05$. The field ionization rates are known from the calculation and therefore we can extract the autoionization rate. Xe autoionization rates are only known in zero field [11–14]. We can directly calculate the $S_{\mathrm{AI}}$ from the zero field $S$ matrix from our theoretical data; for $M=2$, the autoionizing states attached to the $J_{\mathrm{ion}}=1/2$ threshold with $Q=0$ gives $S_{\mathrm{AI}}=0.21$ which is in good agreement with the fitted result.

It is perhaps surprising that the value of $S_{\mathrm{AI}}$ should turn out to be smaller for this experiment on Xe than our previous experiment on NO ($S_{\mathrm{AI}}=0.25$). On average, the predissociation rates for NO [15–17] are substantially smaller than the autoionization rates in Xe. This paradox is solved by noting that the current experiment excites very specific Rydberg resonances: $Q$ (the angular momentum that results from coupling the spin of the outer electron to the total angular momentum of the core) must initially be zero. Some of the broadest Xe resonances (for example, the $J=1$ $nd$ series) have $Q=1$. If the experiment would probe $Q=1$ Rydberg states, the observed value of $S_{\mathrm{AI}}$ should increase dramatically (e.g., for the $J_{\mathrm{ion}}=1/2$, $Q=1$ state, $S_{\mathrm{AI}}$ is 7.5).

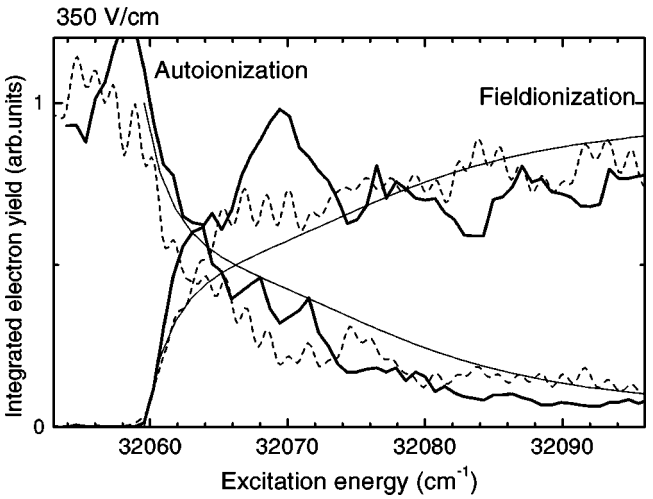


FIG. 6. Integrated electron yield of autoionization (AI) from the $J_{\mathrm{ion}}=1/2$ channel to the $J_{\mathrm{ion}}=3/2$ channel versus field ionization (FI) in the $J_{\mathrm{ion}}=1/2$ channel as a function of the energy of one red and one Nd:YAG photon of 18 790 $\mathrm{cm}^{-1}$. The spectra are convoluted with a Gaussian of 1 $\mathrm{cm}^{-1}$. The electric field is 350 V/cm (saddle point at 32 060 $\mathrm{cm}^{-1}$). The dotted line is the simulation based on a full quantum calculation. The thin solid lines are the overall behavior based on Eqs. (2) and (3) with $S_{\mathrm{AI}}=0.17$ and $|D_{\mathrm{AI}}|^2=0.05$.

The $S_{\mathrm{AI}}$ value is a constant for the xenon atom for a given $Q$ channel, independent of excitation energy and the field strength. To demonstrate this, the same experiment was repeated at a lower electric field. In Fig. 6 are shown the AI and FI signals after convolution of 1 $\mathrm{cm}^{-1}$ in a field of 350 V/cm. The saddle point in such a field is at 32 060 $\mathrm{cm}^{-1}$. The dotted lines are the results obtained with a full quantum calculation. The thin solid lines are the overall behavior based on Eqs. (2) and (3), showing again the power of this simplified model. The only parameter that is adjusted in the fit is the new field strength of 350 V/cm, $S_{\mathrm{AI}}$ is kept at 0.17, and $|D_{\mathrm{AI}}|^2=0.05$.

## V. CONCLUSIONS

We have demonstrated the competition between two ionization channels in xenon, field ionization, and autoionization, in the presence of an electric field. Due to the different mechanisms of decay the ratio between the two channels changes from zero at the saddle point to infinity at the zero-field ionization threshold. The overall behavior of the field ionization yield spectrum is dictated in a unique way by the core-dependent autoionization rate. Fitting the field ionization spectrum with some simple formulas derived in Sec. IV allows us to retrieve the total core-dependent decay rate. Since the overall field ionization rate of high Rydberg states of any atom or molecule is the same within a factor of two, depending on the quantum defects, the field ionization spectrum can be used as a clock to find the rate of total core-dependent decay. This general aspect can be very important for systems were it is impossible to detect core-dependent decay directly.

**ACKNOWLEDGMENTS**

The work described in this paper is part of the research program of the FOM (Foundation for Fundamental Research on Matter) and was made possible by the financial support from NWO (Netherlands Organization for the Advancement of Research). F. Robicheaux was supported by the NSF.

[1] J.B.M. Warntjes, F. Robicheaux, J.M. Bakker, and L.D. Noordam, J. Chem. Phys. **111**, 2556 (1999).
[2] D.A. Harmin, Phys. Rev. A **24**, 2491 (1981); **26**, 2656 (1998).
[3] F. Robicheaux, C. Wesdorp, and L.D. Noordam, Phys. Rev. A **60**, 1420 (1999).
[4] C.E. Moore (unpublished).
[5] A. Kohlhase and S. Kita, Rev. Sci. Instrum. **57**, 2925 (1986).
[6] The more obvious 1+1 excitation with 622 nm shows resonant structure at the one-photon level and is not used.
[7] H. Helm, N. Bjerre, M.J. Dyer, D.L. Huestis, and M. Saeed, Phys. Rev. Lett. **70**, 3221 (1993).
[8] A.T.J. Eppink and D.H. Parker, Rev. Sci. Instrum. **68**, 3477 (1997).
[9] C. Nicole, I. Sluimer, F. Rosca-Pruna, J.B.M. Warntjes, M. Vrakking, C. Bordas, F. Texier, and F. Robicheaux (unpublished).
[10] The rings correspond to excitation with two times Nd:YAG plus one red photon and three times Nd:YAG starting with the $6s$ $(J=2)$ in the $J_{\mathrm{ion}}=3/2$ channel, directly ionizing in the $J_{\mathrm{ion}}=1/2$ channel. The resonance is a coupling of a virtual level at two times Nd:YAG starting from the $6s$ $(J=2)$ state in the $J_{\mathrm{ion}}=3/2$ channel minus one red photon to the $5d'$ state $(J=2)$ in the $J_{\mathrm{ion}}=1/2$ channel at 91 448 $\mathrm{cm}^{-1}$. The ring corresponding to the two times Nd:YAG plus one red photon starting from the $J_{\mathrm{ion}}=3/2$ channel is almost on top of the AI ring in the radial distribution. Therefore there is an increase in electron yield in its integration window not related to the competition between AI and FI.
[11] L. Wang and R.D. Knight, Phys. Rev. A **34**, 3902 (1986).
[12] K. Maeda, K. Ueda, and K. Ito, J. Phys. B **26**, 1541 (1993); Phys. Rev. A **45**, 527 (1992).
[13] M.J.J. Vrakking and Y.T. Lee, J. Chem. Phys. **102**, 8833 (1995).
[14] W.E. Ernst, T.P. Softley, and R.N. Zare, Phys. Rev. A **37**, 4172 (1988).
[15] M.J.J. Vrakking, J. Chem. Phys. **105**, 7336 (1996).
[16] A. Fujii and N. Morita, J. Chem. Phys. **103**, 6029 (1995); **98**, 4581 (1993); Laser Chem. **13**, 259 (1994).
[17] S.T. Pratt, J. Chem. Phys. **108**, 7131 (1998).